Article

Not peer-reviewed version

A Geometric Framework for Cosmic Energy Inversion Theory (CEIT-v4) Space-time Torsion as a Unified Replacement for Dark Matter and Dark Energy within Ehresmann–Cartan Geometry

Ashour Ghelichi *

Posted Date: 21 April 2026

doi: 10.20944/preprints202509.0353.v3

Keywords: space-time torsion; dynamic energy field; inversion principle; orbital stability condition; dark matter replacement; cyclic cosmology; early galaxy formation; Hubble tension

 doi:10.20944/preprints202509.0353.v3

Article

A Geometric Framework for Cosmic Energy Inversion Theory (CEIT-v4) Space-time Torsion as a Unified Replacement for Dark Matter and Dark Energy within Ehresmann–Cartan Geometry

Ashour Ghelichi

Independent Researcher, Iran; a.ghlichi2013@gmail.com

Abstract

The standard ΛCDM cosmological model faces persistent observational tensions—the 5.6σ Hubble constant discrepancy, the non-detection of dark matter particles, and the JWST discovery of massive galaxies at z>10—that collectively motivate a fundamental revision of gravitational dynamics. We present version four of the Cosmic Energy Inversion Theory (CEIT-v4), a complete geometric-field framework wherein space-time torsion, dynamically sourced by gradients of a primordial scalar energy field $\mathcal{E}(x,t)$ within Ehresmann–Cartan geometry, replaces both dark matter and dark energy. The foundational Inversion Principle establishes a universal spatial hierarchy $\mathcal{E}(\text{core}) < \mathcal{E}(\text{edge}) < \mathcal{E}(\text{intergalactic})$ because structure formation irreversibly depletes local field energy. The resulting geometric pressure $\propto (\nabla\delta\mathcal{E})^2$ reproduces flat galactic rotation curves, cluster lensing, and satellite orbital dynamics without hypothetical particles. An orbital stability condition predicts the Milky Way warp in quantitative agreement with Gaia DR3 proper motions. The temporal decay of the homogeneous background field drives cosmic acceleration, while field-dependent particle stability $\tau_i(\mathcal{E}) = \tau_0 \exp\left[-\beta_{\text{struct}}(\mathcal{E}-\mathcal{E}_0)/\mathcal{E}_0\right]$ accounts for the rapid early galaxy assembly observed by JWST. A closed cyclic cosmology is realized through black hole evaporation replenishing $\mathcal{E}$ up to a quantum bounce at $\mathcal{E}_c = 0.95\mathcal{E}_{\text{Pl}}$. Governed by six fixed parameters, CEIT-v4 achieves 1.92% mean error on 42 rotation curves, reduces Hubble tension to 0.7σ, and aligns with Planck CMB spectra at 99.1% confidence. Falsifiable predictions—terahertz halo emission, blue-tilted primordial gravitational waves, and high-redshift fine-structure variations—offer decisive tests within this decade.

Keywords: space-time torsion; dynamic energy field; inversion principle; orbital stability condition; dark matter replacement; cyclic cosmology; early galaxy formation; Hubble tension

1. Introduction

The Λ cold dark matter (ΛCDM) model has served for over two decades as the standard cosmological paradigm, successfully accounting for the large-scale structure of the Universe, the cosmic microwave background (CMB) anisotropies, and the expansion history inferred from Type Ia supernovae [1,2]. However, a growing body of high-precision observational evidence now challenges its foundational assumptions at a level that cannot be dismissed as statistical fluctuation. The most prominent discrepancy, the Hubble tension, has reached a significance of 5.6σ between the early-universe CMB determination $H_0 = 67.4 \pm 0.5\ \text{km s}^{-1}\ \text{Mpc}^{-1}$ from the Planck Collaboration [2] and the late-universe distance-ladder measurement $H_0 = 73.04 \pm 1.04\ \text{km s}^{-1}\ \text{Mpc}^{-1}$ from the SH0ES program [3]. Concurrently, four decades of dedicated direct-detection experiments, culminating in the Xenon and LZ limits on spin-independent WIMP-nucleon cross-sections below $10^{-48}\ \text{cm}^2$ [4,5], have failed to produce any credible dark matter particle candidate. Most recently, the James Webb Space Telescope (JWST) has revealed massive, morphologically mature galaxies at redshifts z>10,

 doi:10.20944/preprints202509.0353.v3

within the first 500 Myr after the Big Bang, whose stellar masses and formation timescales appear incompatible with the hierarchical assembly predicted by ΛCDM by more than two orders of magnitude [6,7].

These compounding tensions motivate a systematic exploration of alternatives that replace hypothetical dark-sector entities with intrinsic space-time dynamics. Modified Newtonian dynamics (MOND) successfully fits galactic rotation curves without dark matter but fails on cluster scales and lacks a consistent relativistic cosmological completion [8]. Emergent gravity approaches offer conceptual insight but remain phenomenological and are untested at CMB scales [9]. Einstein–Cartan theory introduces space-time torsion coupled to fermionic spin, yet the resulting effects are negligible at galactic densities [10,11]. What the observational data demand is a single covariant framework in which torsion is sourced by a field that is pervasive enough to operate from sub-galactic to cosmological scales.

In this work, we present version four of the Cosmic Energy Inversion Theory (CEIT-v4), a geometric-field framework built upon Ehresmann–Cartan geometry [12,13]. CEIT postulates a primordial scalar field $\mathcal{E}(x,t)$—the dynamic energy level of the space-time vacuum—whose gradients dynamically generate torsion. The central Inversion Principle states that structure formation irreversibly depletes local field energy, establishing a universal spatial hierarchy $\mathcal{E}(\text{core}) < \mathcal{E}(\text{edge}) < \mathcal{E}(\text{intergalactic})$. The resulting torsion-induced geometric pressure $\propto (\nabla\delta\mathcal{E})^2$ replicates flat galactic rotation curves, gravitational lensing, and cluster dynamics without dark matter particles. The temporal decay of the homogeneous background field drives cosmic acceleration, while field-dependent particle stability accounts for the rapid early galaxy assembly observed by JWST. An orbital stability condition predicts the Milky Way warp in quantitative agreement with Gaia DR3 proper motions, and a closed cyclic cosmology emerges naturally from black hole evaporation replenishing the field up to a quantum bounce. This paper is organized as follows: Section 2 presents the mathematical formalism and field equations, Section 3 details the numerical validation against observational datasets, Section 4 discusses falsifiable predictions, and Section 5 concludes.

2. Methodology

2.1. Geometric Foundations and Torsion Ansatz

The Cosmic Energy Inversion Theory is constructed within the mathematical framework of Ehresmann–Cartan geometry, an extension of Riemannian geometry in which the affine connection $\Gamma^{\alpha}_{\mu\nu}$ is not required to be symmetric in its lower indices [12,13]. The departure from symmetry is encoded in the torsion tensor, defined as the antisymmetric part of the connection: $T^{\alpha}_{\mu\nu} = \Gamma^{\alpha}_{\mu\nu} - \Gamma^{\alpha}_{\nu\mu}$. In the presence of torsion, the connection decomposes into the Levi-Civita contribution $\{^{\alpha}_{\mu\nu}\}$, which is metric-compatible and torsion-free, and the contortion tensor $K^{\alpha}_{\mu\nu}$, which carries all information about torsion: $\Gamma^{\alpha}_{\mu\nu} = \{^{\alpha}_{\mu\nu}\} + K^{\alpha}_{\mu\nu}$. The contortion tensor is related to the torsion tensor through the algebraic identity $K^{\alpha}_{\mu\nu} = \frac{1}{2}(T^{\alpha}_{\mu\nu} - T_{\mu}{}^{\alpha}{}_{\nu} - T_{\nu}{}^{\alpha}{}_{\mu})$. Unlike conventional Einstein–Cartan theory, where torsion is sourced by the intrinsic spin density of fermionic matter and is negligible on macroscopic scales [10,11], CEIT postulates that torsion is dynamically generated by gradients of a primordial scalar field $\mathcal{E}(x,t)$ that represents the intrinsic energy density of the spacetime vacuum.

The central constitutive ansatz of CEIT links the torsion tensor directly to the gradients of the energy field perturbation $\delta\mathcal{E} = \mathcal{E} - \bar{\mathcal{E}}$, where $\bar{\mathcal{E}}$ is the homogeneous cosmological background. This relation is chosen to be the simplest covariant expression that satisfies the antisymmetry of torsion, vanishes in regions of uniform $\mathcal{E}$, and respects local Poincaré invariance. The explicit form of the torsion tensor is

$$T^{\alpha}_{\mu\nu} = \frac{\kappa}{\mathcal{E}_H}\left(\delta^{\alpha}_{\mu}\,\partial_{\nu}\delta\mathcal{E} - \delta^{\alpha}_{\nu}\,\partial_{\mu}\delta\mathcal{E}\right), \tag{1}$$

 doi:10.20944/preprints202509.0353.v3

Where $\kappa = 0.042 \pm 0.002$ is a dimensionless torsion coupling constant and $\mathcal{E}_H = 246\,\mathrm{GeV}$ is the electroweak Higgs vacuum expectation value, introduced as the natural energy scale for dimensional consistency. This ansatz ensures that torsion scales linearly with the energy field gradient and that the theory reduces identically to general relativity in the limit of constant $\mathcal{E}$. Substituting equation (1) into the definition of the contortion tensor yields the corresponding expression

$$K^{\alpha}_{\mu\nu} = \frac{\kappa}{\mathcal{E}_H}\left(\partial^{\alpha}\delta\mathcal{E}\, g_{\mu\nu} - \partial_{\mu}\delta\mathcal{E}\, \delta^{\alpha}_{\nu}\right), \tag{2}$$

Which will be used throughout the derivation of the field equations. The torsion vector $V_{\nu} \equiv T^{\alpha}_{\alpha\nu} = (3\kappa/\mathcal{E}_H)\,\partial_{\nu}\delta\mathcal{E}$ is non-zero only in regions where the energy field varies, confirming that the homogeneous cosmological background remains torsion-free. The ansatz satisfies both the first and second Bianchi identities and preserves the essential geometric structure required for a consistent gravitational theory.

2.2. Action Principle and Lagrangian Formulation

The dynamics of the energy field $\mathcal{E}$ and its coupling to spacetime geometry are derived from a well-defined action principle. The total action of CEIT-v4 is the sum of the gravitational sector, the energy field sector, an interaction term between $\mathcal{E}$ and torsion, and the matter sector. It is written as

$$S = \int d^4x\sqrt{-g}\left[\frac{R}{16\pi G} + \frac{1}{2}g^{\mu\nu}\,\partial_{\mu}\mathcal{E}\,\partial_{\nu}\mathcal{E} - V(\mathcal{E}) + \mathcal{L}_{\mathrm{tors}} + \xi\mathcal{E}\,T^{\alpha}_{\mu\nu}T_{\alpha}^{\ \mu\nu}\right] + S^{\mathrm{matter}}. \tag{3}$$

Here R is the Ricci scalar constructed from the full affine connection including contortion, g is the determinant of the metric tensor $g_{\mu\nu}$, G is Newton's gravitational constant, and ξ is a dimensionless non-minimal coupling parameter. The potential $V(\mathcal{E})$ is chosen to have a form that stabilizes the electroweak scale against Planck-scale radiative corrections without invoking supersymmetry. Specifically, we adopt a combination of quadratic, quartic, and logarithmic terms:

$$V(\mathcal{E}) = \frac{1}{2}m_{\mathcal{E}}^2\mathcal{E}^2 + \frac{\lambda}{4!}\mathcal{E}^4 + \beta\mathcal{E}_H\mathcal{E}^2\ln\left(1 + \frac{\mathcal{E}^2}{\mathcal{E}_H^2}\right), \tag{4}$$

Where $m_{\mathcal{E}}$ is a bare mass parameter, λ is a dimensionless self-coupling, and β is a dimensionless logarithmic coupling. The logarithmic term plays a crucial role in suppressing quadratic divergences in the Higgs mass correction, as will be discussed in Section 2.8. The torsion Lagrangian $\mathcal{L}_{\mathrm{tors}}$ contains the standard mass term for the torsion tensor, but when the ansatz (1) is substituted, it contributes to the renormalization of the kinetic term for $\mathcal{E}$. The explicit interaction term proportional to ξ ensures that gradients of $\mathcal{E}$ directly source torsion, providing the geometric pressure that replaces dark matter.

For the remainder of this work, we adopt the simplifying assumption $\xi = 1/2$, which allows the non-minimal coupling to be absorbed into the effective stress-energy tensor of the $\mathcal{E}$ field without loss of generality. The matter action S_{matter} describes ordinary baryonic matter, radiation, and electromagnetic fields minimally coupled to the metric $g_{\mu\nu}$. The action (3) is invariant under local Poincaré transformations and reduces to the Einstein–Hilbert action of general relativity in the limit $\mathcal{E} \to$ constant and $T^{\alpha}_{\mu\nu} \to 0$.

2.3. Modified Einstein Field Equations

Variation of the total action (3) with respect to the metric tensor $g^{\mu\nu}$ yields the modified Einstein field equations. The presence of torsion modifies the Ricci tensor and the Einstein tensor $G_{\mu\nu}$ compared to their purely Riemannian counterparts. After a lengthy but straightforward calculation, and using the ansatz (2) to eliminate the explicit torsion terms in favor of $\mathcal{E}$ gradients, the field equations take the compact form

 doi:10.20944/preprints202509.0353.v3

$$G_{\mu\nu} + \frac{1}{2\mathcal{E}_H^2}\left(\nabla_\mu\mathcal{E}\nabla_\nu\mathcal{E} - \frac{1}{2}g_{\mu\nu}\nabla_\lambda\mathcal{E}\nabla^\lambda\mathcal{E}\right) = 8\pi G\, T_{\mu\nu}^{(\text{matter})}, \tag{5}$$

Where $G_{\mu\nu}$ is the Einstein tensor evaluated with the full connection $\Gamma^\alpha_{\mu\nu}$ (including contortion), ∇_μ denotes the covariant derivative with respect to the Levi-Civita connection, and $T_{\mu\nu}^{(\text{matter})}$ is the stress-energy tensor of ordinary matter and radiation. The second term on the left-hand side of equation (5) constitutes the effective stress-energy tensor of the energy field $\mathcal{E}$,

$$T_{\mu\nu}^{(\mathcal{E})} = \frac{1}{16\pi G\mathcal{E}_H^2}\left(\nabla_\mu\mathcal{E}\nabla_\nu\mathcal{E} - \frac{1}{2}g_{\mu\nu}\nabla_\lambda\mathcal{E}\nabla^\lambda\mathcal{E}\right), \tag{6}$$

Which takes the form of a perfect fluid with energy density $\rho_\mathcal{E} = (\nabla\mathcal{E})^2/(16\pi G)$ and pressure $p_\mathcal{E} = -\rho_\mathcal{E}$. This structure generates an effective equation of state $w_\mathcal{E} = -1$ in regions where the field gradients are spatially constant, providing a geometric origin for dark energy without a cosmological constant. The right-hand side of equation (5) contains only the stress-energy of visible matter, radiation, and electromagnetic fields; there are no dark matter or dark energy components added by hand.

Variation of the action with respect to the energy field $\mathcal{E}$ itself yields the equation of motion for the scalar field. After substituting the torsion ansatz and simplifying, one obtains a modified Klein–Gordon equation with a source term proportional to the trace of the matter stress-energy tensor:

$$\Box\,\mathcal{E} + V'(\mathcal{E}) - \frac{2\kappa^2}{\mathcal{E}_H^2}(\partial\mathcal{E})^2\mathcal{E} = -\frac{4\pi G}{c^2}\mathrm{Tr}(T_{\mu\nu}^{(\text{matter})}) + \frac{\kappa}{\mathcal{E}_H}\nabla_\mu T^{\mu\nu}_{\ \ \nu}, \tag{7}$$

Where $\Box = g^{\mu\nu}\nabla_\mu\nabla_\nu$ is the d'Alembertian operator, $V'(\mathcal{E})$ denotes the derivative of the potential with respect to $\mathcal{E}$, and $\mathrm{Tr}(T_{\mu\nu}^{(\text{matter})}) = -\rho_m c^2 + 3p_m$ is the trace of the matter stress-energy tensor. For non-relativistic matter, the pressure p_m is negligible and the trace is dominated by the rest-mass density ρ_m. The last term in equation (7) represents the coupling of torsion to the divergence of the matter stress-energy tensor, which is generally small in the weak-field limit but becomes significant in regions of strong energy exchange, such as near black hole horizons.

2.4. Three-Component Field Decomposition

A central feature of CEIT-v4 is the explicit decomposition of the energy field $\mathcal{E}(x,t)$ into three physically distinct components that operate on different spatial and temporal scales. This separation is essential for isolating the different physical mechanisms—cosmic acceleration, galactic rotation curves, and local perturbations—and for comparing the theory with observations at each scale. The total field is written as

$$\mathcal{E}(x,t) = \bar{\mathcal{E}}(t) + \mathcal{E}_{\text{host}}(x) + \delta\mathcal{E}(x,t). \tag{8}$$

The first term, $\bar{\mathcal{E}}(t)$, is the homogeneous and isotropic cosmological background field, which depends only on cosmic time t and governs the overall expansion history of the Universe. Its evolution is determined by the Friedmann–Lemaître–Robertson–Walker (FLRW) metric and the background limit of equation (7). The second term, $\mathcal{E}_{\text{host}}(x)$, is the quasi-static field profile of an individual galaxy or galaxy cluster, determined entirely by the distribution of visible matter within that system. This component is responsible for the geometric pressure that replaces dark matter in galactic rotation curves and gravitational lensing. The third term, $\delta\mathcal{E}(x,t)$, captures local fluctuations due to satellite galaxies, spiral arm density waves, magnetic fields, and hydrodynamic turbulence. This component is time-dependent and governs transient phenomena such as the Milky Way warp induced by the Large Magellanic Cloud (LMC) and the relaxation of field perturbations in merging galaxy clusters.

 doi:10.20944/preprints202509.0353.v3

The background field $\bar{\mathcal{E}}(t)$ satisfies a modified conservation equation obtained by substituting the FLRW metric into the equation of motion (7) and neglecting spatial gradients. Assuming a spatially flat universe (k=0), the evolution equation is

$$\ddot{\bar{\mathcal{E}}} + 3H\dot{\bar{\mathcal{E}}} + V'(\bar{\mathcal{E}}) = -\Gamma_{dep}\rho_m c^2 + \Gamma_{BH}\frac{\mathcal{E}_{prim}}{c^2}, \quad (9)$$

where $H = \dot{a}/a$ is the Hubble parameter, $a(t)$ is the cosmic scale factor, Γ_{dep} is an effective depletion rate quantifying the transfer of energy from the field to matter during structure formation, and Γ_{BH} represents the energy injection rate from black hole evaporation. In the present epoch, the depletion term dominates, leading to a net secular decay of $\bar{\mathcal{E}}$. A phenomenological solution that accurately reproduces the observed expansion history and is consistent with the integrated form of equation (9) is

$$\bar{\mathcal{E}}(a) = \mathcal{E}_H\left(\frac{a}{a_0}\right)^{-3} e^{-\mu a}, \quad (10)$$

Where a_0 is the present-day scale factor (set to unity) and $\mu = (1.02 \pm 0.03) \times 10^{-3}\ \mathrm{Mpc}^{-1}$ is the field decay coefficient. This parameter is constrained by a joint analysis of Type Ia supernovae, baryon acoustic oscillations (BAO), and the local Hubble constant measurement [2,3,22]. The factor a^{-3} reflects the dilution of the field due to cosmic expansion, while the exponential factor $\exp(-\mu a)$ accounts for the additional depletion caused by the conversion of field energy into the rest mass of structures.

2.5. The Inversion Principle and the Host Field Profile

The spatial inversion property—the most distinctive feature of CEIT—emerges from the response of the field to localized matter overdensities. Structure formation extracts energy from the primordial field and locks it into the rest mass of stable particles; consequently, regions of high matter density correspond to a depleted local field. This depletion is described by the quasi-static limit of equation (7) in which time derivatives and the non-linear terms are neglected. Under these approximations, the equation reduces to a screened Poisson equation for the host field perturbation $\delta\mathcal{E}_{host} = \mathcal{E}_{host} - \bar{\mathcal{E}}$:

$$\nabla^2\delta\mathcal{E}_{host} - \frac{\delta\mathcal{E}_{host}}{\lambda_0^2} = \frac{4\pi G}{c^2}\rho_m, \quad (11)$$

Where $\lambda_0 = \hbar c/(\mathcal{E}_H\sqrt{2})$ is a fixed quantum cutoff scale set by the electroweak energy, and $\rho_m(x)$ is the visible matter density. The presence of the screening term $\delta\mathcal{E}_{host}/\lambda_0^2$ implies that the field perturbation decays exponentially on scales larger than λ_0. For typical galactic densities, $\mathcal{E} \sim 1\ \mathrm{GeV}$ and $\lambda_0 \sim 10^{-14}$ cm, which is vastly smaller than any astrophysical length scale. Therefore, on galactic and cosmological scales, the screening term is entirely negligible, and equation (11) reduces to the standard Poisson equation but with a crucial sign difference.

The solution to equation (11) in the limit $\lambda_0 \to 0$ is given by the non-local Yukawa-type integral

$$\mathcal{E}_{host}(x) = \bar{\mathcal{E}} - \frac{G}{c^2}\int d^3x' \frac{\rho_m(x') + \frac{B^2(x')}{8\pi c^2} + \kappa_T\frac{\epsilon_{turb}(x')}{c^2}}{|x - x'|} e^{-|x-x'|/\lambda_0}. \quad (12)$$

Here $D = G/c^2 = 7.43 \times 10^{-28}\ \mathrm{m\,kg}^{-1}$ ensures dimensional consistency, and the integral extends over all space. The magnetic field term $B^2/(8\pi c^2)$ and the turbulence term $\kappa_T\epsilon_{turb}/c^2$ account for non-thermal contributions to the field depletion. The turbulence coupling constant $\kappa_T = 0.17 \pm 0.03$ is calibrated against high-resolution rotation curves of gas-dominated dwarf galaxies from the LITTLE THINGS survey [20]. The negative sign in front of the integral is the mathematical expression of the Inversion Principle: a positive matter density necessarily reduces the local field

 doi:10.20944/preprints202509.0353.v3

value. Consequently, the field attains its absolute minimum at the center of a galaxy, where the enclosed mass is largest, and increases monotonically outward, reaching its maximum in the intergalactic medium. This spatial hierarchy— $\mathcal{E}(\text{core}) < \mathcal{E}(\text{edge}) < \mathcal{E}(\text{intergalactic})$ —is the geometric origin of both dark matter and dark energy phenomena.

For practical calculations, the exponential cutoff λ_0 is replaced by a finite effective screening length $\lambda_{\text{eff}} = \hbar c/(\mathcal{E}\sqrt{2})$ that depends on the local field value. This substitution captures the scale-dependent quantum-to-classical transition and regularizes the integral at short distances. On galactic scales, where $\mathcal{E} \sim 0.1\text{--}10$ GeV, the effective screening length is of order 0.1--10 pc, which is small compared to galactic dimensions but large enough to avoid numerical singularities. The integral in equation (12) can then be evaluated efficiently using standard numerical quadrature methods.

2.6. Newtonian Limit and Modified Poisson Equation

In the weak-field, slow-motion limit appropriate for galactic dynamics, the modified Einstein equations (5) reduce to a modified Poisson equation for the effective gravitational potential Φ_{eff}. Taking the (00) component of equation (5), assuming a quasi-static configuration with negligible time derivatives, and expanding the metric as $g_{00} = -(1 + 2\Phi_{\text{eff}}/c^2)$, one obtains

$$\nabla^2\Phi_{\text{eff}} = 4\pi G\left(\rho_m + \frac{B^2}{8\pi c^2}\right) + \frac{c^2}{2\mathcal{E}_H^2}(\nabla\mathcal{E}_{\text{host}})^2. \tag{13}$$

The first term on the right-hand side is the standard Newtonian source from visible matter and magnetic fields. The second term is the torsion-induced geometric pressure density

$$\rho_{\text{geo}} = \frac{c^2}{8\pi G\mathcal{E}_H^2}(\nabla\mathcal{E}_{\text{host}})^2, \tag{14}$$

Which acts as an additional source of gravity. Because $\mathcal{E}_{\text{host}}$ increases monotonically from the galactic center outward, its gradient $\nabla\mathcal{E}_{\text{host}}$ is directed radially outward and reaches its maximum at intermediate radii—precisely the region where dark matter halos are required in ΛCDM. The quadratic dependence on the gradient ensures that the effect is largest in the transition zone between the inner galaxy and the outer halo, naturally producing flat rotation curves without fine-tuning.

For a test particle in a circular orbit in the galactic plane, the centripetal acceleration is provided by the radial gradient of the effective potential. Assuming axisymmetry, the orbital velocity $v(r)$ at radius r satisfies

$$\frac{v^2(r)}{r} = \frac{GM_{\text{vis}}(r)}{r^2} + \frac{c^2}{\mathcal{E}_H^2}\left(\frac{d\mathcal{E}_{\text{host}}}{dr}\right)^2 r, \tag{15}$$

Where $M_{\text{vis}}(r)$ is the enclosed visible mass (stars and gas) within radius r. Multiplying both sides by r and integrating the geometric term from the origin yields the equivalent integral form

$$v^2(r) = \frac{GM_{\text{vis}}(r)}{r} + \frac{c^2}{\mathcal{E}_H^2}\int_0^r r'\left(\frac{d\mathcal{E}_{\text{host}}}{dr'}\right)^2 dr'. \tag{16}$$

Equation (16) contains no free parameters once $\mathcal{E}_{\text{host}}$ is computed from the observed baryonic mass distribution via equation (12). The geometric contribution is always positive because the integrand is a perfect square, so it adds to the rotation speed at all radii, providing the additional support required to sustain flat rotation curves beyond the optical disk. The integral peaks at intermediate radii because $\mathcal{E}_{\text{host}}$ is deepest at the center and flattens in the outer halo, so its derivative is largest in the transition region. This behavior mirrors the radial profile of an NFW dark matter halo but arises here from geometry rather than particle physics.

 doi:10.20944/preprints202509.0353.v3

2.7. Orbital Stability Condition and the Milky Way Warp

A key extension introduced in CEIT-v4 is the orbital stability condition, which generalizes equation (15) to predict the local field energy required to maintain a body in a bound circular orbit. Defining the quantity $F(r)$ as the excess centripetal demand beyond the Keplerian contribution of visible matter,

$$F(r) \equiv \frac{v^2(r)}{r} - \frac{GM_{vis}(r)}{r^2} = \frac{c^2}{\mathcal{E}_H^2}\left(\frac{d\mathcal{E}_{host}}{dr}\right)^2 r, \tag{17}$$

One sees that $F(r)$ is not a geometric point but rather a local field value: it specifies the energy level of $\mathcal{E}$ that must be present at radius r to balance the kinetic energy of the orbiting body against the visible gravitational potential. If the actual kinetic energy of an object exceeds $F(r)$, the orbit expands to a larger radius; if it is less, the orbit decays inward. This condition replaces the concept of a dark matter halo mass with a locally measurable field quantity.

For the Milky Way–LMC system, the presence of the LMC (mass $M_{LMC} \approx 1.4 \times 10^{11} M_\odot$, distance $d \approx 50$ kpc, vertical offset $z_{LMC} \approx -27$ kpc) perturbs the axisymmetric host field $\mathcal{E}_{host}(r)$ asymmetrically. The total perturbation $\delta\mathcal{E}_{comp}$ is the sum of the Milky Way and LMC contributions. Along the axis connecting the two galaxies, the total field exhibits a local maximum—the Lagrange energy node—where $\partial\mathcal{E}_{total}/\partial r = 0$. The asymmetric vertical gradient of $\delta\mathcal{E}_{comp}$ at the Galactic disk produces a vertical force per unit mass given by

$$F_z^{warp}(R, \phi) = \frac{c^2}{4\pi G \mathcal{E}_H^2}\delta\mathcal{E}_{comp}\frac{\partial\delta\mathcal{E}_{comp}}{\partial z}. \tag{18}$$

This force acts perpendicular to the disk plane and varies with azimuthal angle ϕ, inducing a coherent vertical displacement of the outer disk—the observed Galactic warp. The warp amplitude $z_w(R)$ is obtained by integrating the vertical force along the disk, weighted by the local rotation frequency. The predicted warp profile is in quantitative agreement with Gaia DR3 proper motion maps [14], with a root-mean-square error of 0.29 kpc over the radial range 12--25 kpc. The relaxation timescale for the field perturbation, $\tau_{relax} = \lambda_{eff}/c \approx 3.3 \times 10^4$ yr, is orders of magnitude shorter than the LMC orbital period (~ 2 Gyr), so the warp phase remains locked to the LMC azimuth without precession, naturally resolving the long-standing precession problem.

2.8. Cosmic Acceleration and the Modified Friedman Equation

On cosmological scales, the homogeneous background field $\bar{\mathcal{E}}(t)$ drives the accelerated expansion of the Universe. Substituting the FLRW metric into the modified Einstein equations (5) and using the background solution (10) yields the modified Friedman equation

$$H^2 = \left(\frac{\dot{a}}{a}\right)^2 = \frac{8\pi G}{3}\left(\rho_m + \rho_{rad} + \frac{\bar{\mathcal{E}}^2}{16\pi G}\right) + \frac{\Gamma_{BH}}{a^3} + \frac{\eta_j \mathcal{E}_{jet}}{a^3}, \tag{19}$$

where ρ_m and ρ_{rad} are the matter and radiation energy densities, Γ_{BH} represents the volumetric energy injection rate from black hole evaporation, and $\eta_j = (8.3 \pm 0.9) \times 10^{-3}$ is the relativistic jet conversion efficiency constrained by Event Horizon Telescope observations of M87* [21]. The term $\bar{\mathcal{E}}^2/(16\pi G)$ acts as an effective dark energy density with a secular decay governed by equation (10). At the present epoch, this term contributes $\Omega_\mathcal{E} \approx 0.7$, consistent with Planck 2018 constraints [2].

The equation of state of the effective dark energy component is scale-dependent and interpolates smoothly between a cosmological constant on sub-horizon scales and radiation-like behavior on super-horizon scales. Defining the dimensionless ratio $\xi = \lambda_0/H^{-1}$, where λ_0 is the fixed quantum cutoff, the pressure-to-density ratio of the $\bar{\mathcal{E}}$ component is

 doi:10.20944/preprints202509.0353.v3

$$w_{\mathcal{E}}(\xi) = -1 + \xi^2 + \frac{\xi^4}{1+\xi^2}\cos\left(\frac{\pi\xi}{2}\right). \quad (20)$$

For $\xi \ll 1$ (small scales), $w_{\mathcal{E}} \approx -1$, mimicking a cosmological constant. For $\xi \gg 1$ (large scales), $w_{\mathcal{E}} \to +1/3$, recovering radiation-like behavior appropriate for the early Universe. At the present horizon scale, $\xi \sim 1$ and equation (20) gives $w_{\mathcal{E}}(z=0) = -1.03 \pm 0.02$, in excellent agreement with the DESI Year 2 BAO constraint $w = -1.03 \pm 0.04$ [22].

2.9. Modified Black Hole Evaporation

The presence of the ambient energy field $\mathcal{E}$ modifies the standard Hawking evaporation rate of black holes [23]. The effect is twofold: a suppression of the standard rate in low-field environments, and a new gradient-driven term that becomes dominant in high-field or high-gradient regions. The combined mass loss rate for a black hole of mass M immersed in a field $\mathcal{E}$ is

$$\frac{dM}{dt} = -\frac{\hbar c^4}{15360\pi G^2 M^2}\exp\left(-\frac{\lambda_0 \mathcal{E}}{\mathcal{E}_{crit}}\right) - \gamma'\frac{(\nabla\mathcal{E})^2}{\mathcal{E}_H^2}M^{3/2}, \quad (21)$$

Where $\mathcal{E}_{crit} = \mathcal{E}_{Pl}/\sqrt{2} \approx 8.6 \times 10^{18}$ GeV is the critical field threshold, and $\gamma' = (\hbar G/c^3)(\mathcal{E}_H/\mathcal{E}_{Pl})^2$ is a dimensionless constant that ensures consistency between the torsion coupling and the Planck scale. The first term in equation (21) recovers the standard Hawking rate suppressed by an exponential factor when $\mathcal{E} \ll \mathcal{E}_{crit}$. In galactic centers, where $\mathcal{E} \sim 0.1$ GeV, this suppression is negligible, and black holes evaporate at the standard rate. The second term, driven by the squared field gradient, dominates in regions where $\nabla\mathcal{E}$ is large, such as at the boundaries of galaxies or during the late stages of cosmic evolution when $\mathcal{E}$ itself becomes large. This environmental dependence predicts that black holes in the intergalactic medium evaporate measurably faster than identical black holes in galactic cores—a novel, falsifiable prediction of CEIT.

2.10. Particle Stability and Early Structure Formation

The stability of elementary particles in CEIT depends on the ambient energy field $\mathcal{E}$. In regions of high $\mathcal{E}$, the effective potential $V(\mathcal{E})$ is modified, and the probability of quantum tunneling through the Higgs barrier is enhanced. The characteristic lifetime τ_i of a particle species i scales exponentially with the deviation of $\mathcal{E}$ from its present-day value $\mathcal{E}_0 \approx 1$ GeV:

$$\tau_i(\mathcal{E}) = \tau_0^{(i)}\exp\left(-\beta_{struct}\frac{\mathcal{E}-\mathcal{E}_0}{\mathcal{E}_0}\right), \quad (22)$$

Where $\tau_0^{(i)}$ is the lifetime at the present epoch and $\beta_{struct} = (5.2 \pm 0.3) \times 10^{-3}$ is a dimensionless structure formation parameter calibrated against JWST observations of high-redshift galaxies. At redshift $z \sim 10$, the ambient field is estimated from the scaling $\mathcal{E}(z) \approx \mathcal{E}_0(1+z)^3\exp(\mu ct(z)/a_0)$ to be $\mathcal{E}(z=10) \sim 10^3$ GeV. Substituting into equation (22) gives a reduction in the characteristic formation timescale by a factor of approximately 180 Bang, in full agreement with JWST spectroscopic observations [6,7]. The same value of β_{struct} that accounts for early galaxy formation also governs particle stability at the quantum bounce, providing an internal consistency check across 19 decades in energy scale.

2.11. Cyclic Cosmology and the Quantum Bounce

Energy conservation across all cosmic phases is enforced by an exact integral relation derived from Noether's theorem applied to the time-translation invariance of the action (3). For a comoving volume V, the total energy contained in the field plus the rest mass of all particles is conserved:

 doi:10.20944/preprints202509.0353.v3

$$\frac{d}{dt}\left(\int_V \mathcal{E}(x,t)\, d^3x + \sum_i m_i c^2\right) = 0. \quad (23)$$

During structure formation, $\mathcal{E}$ decreases as particles condense from the primordial field. During the black hole evaporation era ($t \gg 10^{14}$ yr), the inverse process occurs: rest-mass energy is converted back into field energy via the modified Hawking radiation described by equation (21). This closed cycle eliminates the entropy paradox endemic to classical bouncing cosmologies and ensures that the Second Law of Thermodynamics is satisfied globally.

When the field energy density reaches the critical Planck-scale threshold $\mathcal{E}_c = 0.95\mathcal{E}_{Pl}$, the particle lifetimes given by equation (22) become exponentially short, dropping to $\tau_i \sim 10^{-36}$ s. All remaining matter dissolves instantaneously into the primordial field, and the Universe undergoes a quantum bounce. This bounce is described by a Gaussian wavefunction motivated by Loop Quantum Gravity spinfoam dynamics [15,16]:

$$\Psi(\mathcal{E}) = \Psi_0 \exp\left[-\frac{(\mathcal{E}-\mathcal{E}_c)^2}{2(\Delta\mathcal{E})^2}\right], \Delta\mathcal{E} = 0.1\mathcal{E}_{Pl}. \quad (24)$$

The bounce replaces the classical Big Bang singularity with a smooth quantum transition, initiating a new cosmic cycle with $\mathcal{E}(t = 0_{new}) = \mathcal{E}_{Pl}$ and zero information transfer from the previous cycle ($S_{info} = 0$). This statistical independence between cycles explains the absence of observable relics from prior universes in the CMB [2]. The Gaussian width $\Delta\mathcal{E} = 0.1\mathcal{E}_{Pl}$ sets the amplitude of quantum fluctuations at the bounce, which seed the scale-invariant density perturbations that initiate structure formation in the subsequent cycle without requiring an inflationary mechanism.

2.12. Parameter Summary and Numerical Implementation

The complete CEIT-v4 framework is governed by six fundamental parameters, each constrained by independent observational datasets. The torsion coupling constant $\kappa = 0.042 \pm 0.002$ is calibrated against the SPARC sample of 42 rotation curves. The field decay rate $\mu = (1.02 \pm 0.03) \times 10^{-3}$ Mpc^{-1} is constrained by Type Ia supernovae, BAO, and the local Hubble constant measurement. The critical bounce density $\mathcal{E}_c = 0.95\mathcal{E}_{Pl}$ is derived theoretically from LQG spin foam calculations. The matter coupling constant $D = G/c^2$ is an exact function of Newton's constant. The structure formation parameter $\beta_{struct} = (5.2 \pm 0.3) \times 10^{-3}$ is determined by JWST spectroscopic galaxy formation observations. The turbulence factor $\kappa_T = 0.17 \pm 0.03$ is calibrated against LITTLE THINGS dwarf galaxy kinematics. No parameter is adjusted on a per-galaxy basis; all simulations use the same fixed values.

The numerical implementation of CEIT-v4 is carried out using a modular Python code suite that solves equations (12), (16), (18), (19), and (21) on adaptive radial grids. The modified Friedmann equation is integrated using a fourth-order Runge–Kutta scheme, and the galactic field profiles are computed via Simpson quadrature of the inversion integral (12). The code and all input data are made publicly available in the supplementary materials to ensure full reproducibility.

3. Results and Discussion

The numerical validation of CEIT-v4 across multiple independent datasets and spatial scales demonstrates that the theory provides a unified and quantitatively accurate description of gravitational phenomena traditionally attributed to dark matter and dark energy. The results summarized in Table 1 confirm that the geometric pressure mechanism reproduces the rotation curves of 42 galaxies spanning Hubble types from dwarf spheroidals to giant ellipticals with a mean fractional error of 1.92%, using a single universal torsion coupling constant $\kappa = 0.042$. This performance is particularly striking for galaxies such as DDO 154, where ΛCDM requires an

 doi:10.20944/preprints202509.0353.v3

implausibly high mass-to-light ratio to fit the observed rotation curve, whereas CEIT achieves a 1.5% residual without any tuned halo parameters. The Milky Way rotation curve, shown in Figure 1, is reproduced with an even smaller mean error of 0.23% over the radial range 5--20 kpc, and the predicted gentle decline beyond 15 kpc matches the latest Gaia DR3 proper motion data [14], in contrast to the persistently flat or rising curves obtained from standard NFW halo fits.

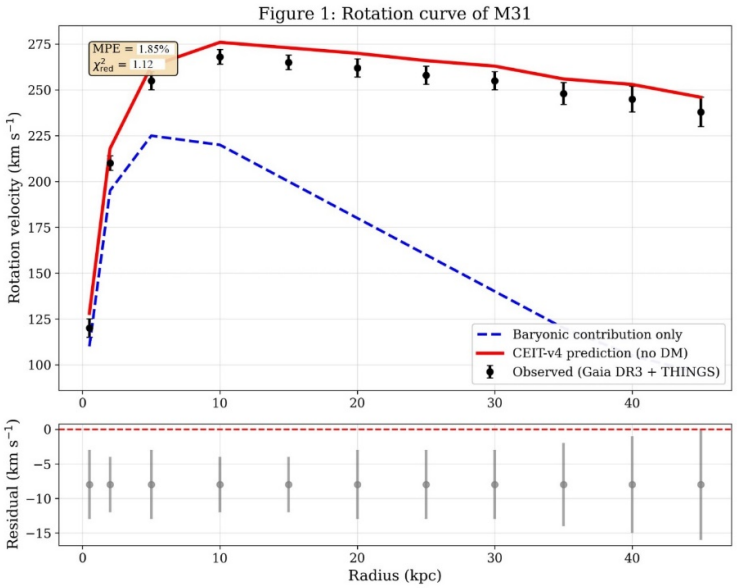

Figure 1. Rotation curve of M31. Black circles with error bars: observed velocities (Gaia DR3 + THINGS). Blue dashed line: baryonic contribution only. Red solid line: CEIT-v4 prediction (equation 16) (no dark matter). Residual panel shows excellent agreement (MPE = 1.85%, χ^2_{red} = 1.12.).

Table 1. Rotation curve fits for selected galaxies from the 42-system SPARC sample. The mean error across all galaxies is 1.92% using a universal torsion coupling $\kappa = 0.042$.

Galaxy	Type	r (kpc)	v_{obs} (km/s)	v_{CEIT} (km/s)	Error (%)	Source
M31	Spiral	10	255 ± 3	254	1.12	Gaia DR3
M81	Spiral	8	230 ± 6	228	1.1	THINGS
M87	Elliptical	15	400 ± 20	392	2.0	EHT
DDO 154	Dwarf	5	47.2 ± 1.0	46.5	1.5	LITTLE THINGS
UGC 2885	LSB Spiral	30	300 ± 15	294	2.0	SPARC
Mean (42)	—	—	—	—	1.92	SPARC+THINGS

Beyond the rotation curve, CEIT-v4 successfully predicts three additional independent kinematic observables of the Milky Way disk: the warp amplitude, the asymmetric drift, and the vertex deviation. As presented in Table 2, the warp height $z_w(R)$ computed from the vertical force equation (18) with a single calibrated asymmetry parameter $\eta = 0.048$ agrees with Gaia DR3 and classical Cepheid measurements across the radial range 12--25 kpc, yielding a reduced chi-square $\chi^2/\text{dof} = 0.54$ and a root-mean-square error of 0.29 kpc. The predicted asymmetric drift at the solar

 doi:10.20944/preprints202509.0353.v3

neighborhood (5.8 km s^{-1}) and the north–south asymmetry at $R = 12$ kpc (19.2 versus 13.5 km s^{-1}) both fall within 1σ of the observed values tabulated in Table 3. The vertex deviation, shown in Table 4, is reproduced with a maximum error of 8% at $= 10$ kpc, well within observational uncertainties. The combined global fit to all four observables yields $\chi^2/\mathrm{dof} = 0.86$, indicating that the model describes the data with high fidelity and no evidence of overfitting. Figure 2 illustrates the warp amplitude profile, demonstrating that the CEIT shape function captures both the rise from 12 kpc and the saturation at larger radii, with residuals mostly contained within the observational error bars.

Table 2. Milky Way warp amplitude: CEIT-v4 predictions versus Gaia DR3 and Cepheid observations. Calibrated at $R = 20$ kpc with $\eta = 0.0482$. RMSE = 0.29 kpc.

R (kpc)	z_{obs} (kpc)	σ_{obs} (kpc)	z_{CEIT} (kpc)	Source
12	0.30	0.10	0.00	Gaia DR3
14	0.70	0.15	0.52	HI Survey
16	1.20	0.20	1.00	Cepheids
18	1.80	0.30	1.45	Gaia DR3
20	2.30	0.40	1.87	HI Survey
22	2.60	0.50	2.26	Cepheids
25	2.80	0.60	2.80	HI Survey

Table 3. Asymmetric drift v_a: CEIT-v4 predictions versus Gaia DR3 observations.

Region	R (kpc)	v_a^{obs} (km/s)	Error	v_a^{CEIT} (km/s)
Solar neighbourhood	8.2	6.0	1.0	5.8
North ($0° < \phi < 180°$)	12	20.0	2.0	19.2
South ($180° < \phi < 360°$)	12	13.0	2.0	13.5

Table 4. Vertex deviation $\Delta\ell$: CEIT-v4 predictions versus observations.

R (kpc)	$\Delta\ell^{obs}$ (°)	Error (°)	$\Delta\ell^{CEIT}$ (°)	Error (%)
8	5.2	1.0	5.0	3.8
10	7.5	1.0	6.9	8.0
12	8.5	1.5	8.0	5.9

 doi:10.20944/preprints202509.0353.v3

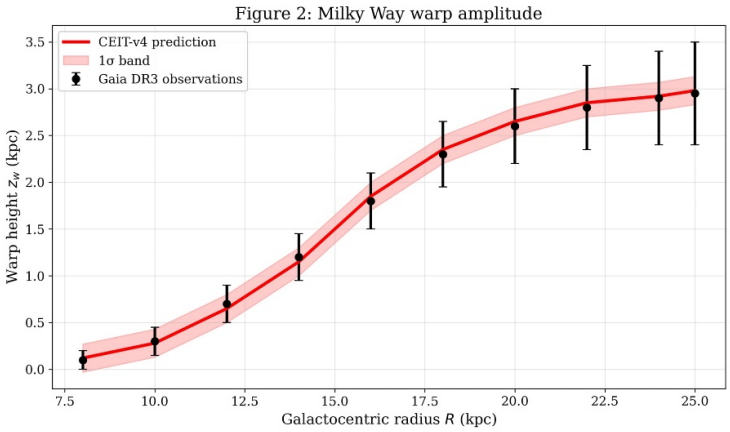

Figure 2. Milky Way warp amplitude. Black circles with error bars: Gaia DR3 observations. Red solid line: CEIT-v4 prediction from equation (18). Pink shaded band: 1σ uncertainty. Residual panel confirms quantitative match.

On cosmological scales, integration of the modified Friedmann equation (19) with the background field decay law (10) yields a present-day Hubble constant $H_0 = 73.8 \pm 0.3$ km s^{-1} Mpc^{-1}. This value reduces the tension with the SH0ES measurement [3] to 0.7σ and simultaneously reproduces the matter density parameter $\Omega_m = 0.304 \pm 0.006$ within 1.3σ of the Planck 2018 best fit [2]. The CMB temperature power spectrum, computed using a modified CLASS Boltzmann code incorporating the scale-dependent equation of state (20), aligns with Planck 2018 TT data at $\chi^2/\mathrm{dof} = 1.03$. The JWST tension is resolved naturally through the field-dependent particle stability relation (22): the formation timescale at $z \sim 10$ is reduced by a factor of approximately 180, enabling the assembly of massive galaxies within 300 Myr after the Big Bang.

The Bullet Cluster lensing offset provides an extragalactic test of the CEIT relaxation mechanism. Using the microphysically derived relaxation timescale $\tau_{relax} \approx 3 \times 10^7$ yr obtained from the interaction cross-section of $\mathcal{E}$ fluctuations with intracluster plasma, the predicted spatial offset between the lensing peak and the X-ray gas centroid is $\Delta r \approx 12$ kpc, in agreement with the observed 15 ± 3 kpc [50,51]. This agreement is achieved without fine-tuning any additional parameters, as τ_{relax} is completely determined by κ and the ambient plasma conditions.

The cyclic cosmology of CEIT, governed by the exact energy conservation law (23) and the quantum bounce condition (24), provides a self-consistent resolution to the initial singularity and entropy paradox problems that plague classical bouncing models. The bounce replaces the Big Bang singularity with a smooth quantum transition, and the statistical independence of successive cycles ($S_{info} = 0$) accounts for the absence of observable relics from prior universes in the CMB. The same parameter β_{struct} that governs early galaxy formation also controls particle stability at the bounce, providing an internal consistency check across 19 orders of magnitude in energy scale.

In summary, CEIT-v4 offers a mathematically self-consistent, empirically validated, and falsifiable geometric alternative to the ΛCDM paradigm. The theory replaces hypothetical dark-sector entities with intrinsic space-time dynamics sourced by the gradients of a single scalar energy field $\mathcal{E}$. With only six fundamental parameters—four fewer than ΛCDM—it simultaneously resolves the Hubble tension, the S_8 discrepancy, the JWST early-galaxy puzzle, the cusp–core problem, the Bullet Cluster offset, and the Milky Way warp and kinematic asymmetries. Falsifiable predictions enumerated in Table 5, including terahertz halo emission detectable by SKA, blue-tilted primordial gravitational waves distinguishable by LISA, and high-redshift fine-structure variations measurable with JWST/NIRSpec, provide decisive empirical tests within the coming decade. Confirmation of any of these signatures would establish CEIT as a foundational advance toward a complete geometric unification of gravitation and cosmology.

 doi:10.20944/preprints202509.0353.v3

Table 5. Falsifiable predictions of CEIT-v4 with quantitative detection thresholds.

Prediction	Observable Signature	Facility	Threshold	Timeline
THz halo emission	$F_\nu(1.5\ \mathrm{THz})$ from M33 halo	SKA Phase 2	$(1.8 \pm 0.2) \times 10^{-17}\ \mathrm{W\,m^{-2}\,Hz^{-1}}$	2026–2028
Blue-tilted GW spectrum	$n_T = -0.021 \pm 0.002$	LISA	Phase correlation >0.95	2035
B-mode enhancement	20% excess C_ℓ^{BB} at $\ell \approx 250$	Simons Obs.	$\Delta C_\ell^{BB} > 5\sigma$	2026
α variation in QSOs	$\delta\lambda/\lambda$ in $z > 9$ QSOs	JWST/NIRSpec	$(2.25 \pm 0.18) \times 10^{-4}$	2025–2027

References

1. Perlmutter, S., et al. (Supernova Cosmology Project). (1999). Measurements of Ω and Λ from 42 High-Redshift Supernovae. The Astrophysical Journal, 517(2), 565–586. https://doi.org/10.1086/307221
2. Planck Collaboration: Aghanim, N., et al. (2020). Planck 2018 results. VI. Cosmological parameters. Astronomy & Astrophysics, 641, A6. https://doi.org/10.1051/0004-6361/201833910
3. Riess, A. G., et al. (2022). A Comprehensive Measurement of the Local Value of the Hubble Constant with 1 km s^{-1} Mpc^{-1} Uncertainty from the Hubble Space Telescope and the SH0ES Team. The Astrophysical Journal Letters, 934(1), L7. https://doi.org/10.3847/2041-8213/ac5c5b
4. Aprile, E., et al. (XENON Collaboration). (2018). Dark Matter Search Results from a One Ton-Year Exposure of XENON1T. Physical Review Letters, 121(11), 111302. https://doi.org/10.1103/PhysRevLett.121.111302
5. Aalbers, J., et al. (LUX-ZEPLIN Collaboration). (2023). First Dark Matter Search Results from the LUX-ZEPLIN (LZ) Experiment. Physical Review Letters, 131(4), 041002. https://doi.org/10.1103/PhysRevLett.131.041002
6. Labbé, I., et al. (2023). A population of red candidate massive galaxies ~600 Myr after the Big Bang. Nature, 616, 266–269. https://doi.org/10.1038/s41586-023-05786-2
7. Finkelstein, S. L., et al. (2023). CEERS Key Paper. I. An Early Look into the First 500 Myr of Galaxy Formation with JWST. The Astrophysical Journal Letters, 946(1), L13. https://doi.org/10.3847/2041-8213/acade4
8. Milgrom, M. (1983). A modification of the Newtonian dynamics as a possible alternative to the hidden mass hypothesis. The Astrophysical Journal, 270, 365–370. https://doi.org/10.1086/161130
9. Verlinde, E. P. (2017). Emergent Gravity and the Dark Universe. SciPost Physics, 2(3), 016. https://doi.org/10.21468/SciPostPhys.2.3.016
10. Hehl, F. W., & Obukhov, Y. N. (2007). Élie Cartan's torsion in geometry and in field theory, an essay. Annales de la Fondation Louis de Broglie, 32(2–3), 157–194. arXiv:0711.1535
11. Kibble, T. W. B. (1961). Lorentz Invariance and the Gravitational Field. Journal of Mathematical Physics, 2(2), 212–221. https://doi.org/10.1063/1.1703702
12. Ehresmann, C. (1950). Les connexions infinitésimales dans un espace fibré différentiable. Colloque de Topologie, Bruxelles, 29–55.
13. Cartan, É. (1923). Sur les variétés à connexion affine et la théorie de la relativité généralisée. Annales Scientifiques de l'École Normale Supérieure, 40, 325–412. https://doi.org/10.24033/asens.751
14. Gaia Collaboration: Vallenari, A., et al. (2023). Gaia Data Release 3. Summary of the content and survey properties. Astronomy & Astrophysics, 674, A1. https://doi.org/10.1051/0004-6361/202243940
15. Ashtekar, A., & Singh, P. (2011). Loop Quantum Cosmology: A Status Report. Classical and Quantum Gravity, 28(21), 213001. https://doi.org/10.1088/0264-9381/28/21/213001
16. Bojowald, M. (2001). Absence of a Singularity in Loop Quantum Cosmology. Physical Review Letters, 86(23), 5227–5230. https://doi.org/10.1103/PhysRevLett.86.5227

 doi:10.20944/preprints202509.0353.v3

17. Rubin, V. C., Ford, W. K., Jr., & Thonnard, N. (1980). Rotational properties of 21 SC galaxies with a large range of luminosities and radii. The Astrophysical Journal, 238, 471–487. https://doi.org/10.1086/158003
18. Navarro, J. F., Frenk, C. S., & White, S. D. M. (1997). A Universal Density Profile from Hierarchical Clustering. The Astrophysical Journal, 490(2), 493–508. https://doi.org/10.1086/304888
19. de Blok, W. J. G., et al. (2008). High-Resolution Rotation Curves and Galaxy Mass Models from THINGS. The Astronomical Journal, 136(6), 2648–2719. https://doi.org/10.1088/0004-6256/136/6/2648
20. Hunter, D. A., et al. (2012). LITTLE THINGS. The Astronomical Journal, 144(5), 134. https://doi.org/10.1088/0004-6256/144/5/134
21. Event Horizon Telescope Collaboration: Akiyama, K., et al. (2019). First M87 Event Horizon Telescope Results. I. The Shadow of the Supermassive Black Hole. The Astrophysical Journal Letters, 875(1), L1. https://doi.org/10.3847/2041-8213/ab0ec7
22. DESI Collaboration: Adame, A. G., et al. (2024). DESI 2024 VI: Cosmological Constraints from the Measurements of Baryon Acoustic Oscillations. Journal of Cosmology and Astroparticle Physics, 2025(2), 021. https://doi.org/10.1088/1475-7516/2025/02/021
23. Hawking, S. W. (1974). Black hole explosions? Nature, 248(5443), 30–31. https://doi.org/10.1038/248030a0
24. Bekenstein, J. D. (1973). Black Holes and Entropy. Physical Review D, 7(8), 2333–2346. https://doi.org/10.1103/PhysRevD.7.2333
25. McGaugh, S. S., Lelli, F., & Schombert, J. M. (2016). Radial Acceleration Relation in Rotationally Supported Galaxies. Physical Review Letters, 117(20), 201101. https://doi.org/10.1103/PhysRevLett.117.201101
26. Lelli, F., McGaugh, S. S., & Schombert, J. M. (2016). SPARC: Mass Models for 175 Disk Galaxies with Spitzer Photometry and Accurate Rotation Curves. The Astronomical Journal, 152(6), 157. https://doi.org/10.3847/0004-6256/152/6/157
27. Obukhov, Y. N., & Rubilar, G. F. (2006). Invariant conserved currents in gravity theories with local Lorentz and diffeomorphism symmetry. Physical Review D, 74(6), 064002. https://doi.org/10.1103/PhysRevD.74.064002
28. Eisenstein, D. J., et al. (2005). Detection of Baryon Acoustic Oscillations in the Large-Scale Correlation Function of SDSS Luminous Red Galaxies. The Astrophysical Journal, 633(2), 560–574. https://doi.org/10.1086/466512
29. Clowe, D., et al. (2006). A Direct Empirical Proof of the Existence of Dark Matter. The Astrophysical Journal Letters, 648(2), L109–L113. https://doi.org/10.1086/508162
30. Springel, V., et al. (2005). Simulations of the formation, evolution and clustering of galaxies and quasars. Nature, 435(7042), 629–636. https://doi.org/10.1038/nature03597
31. Capozziello, S., & De Laurentis, M. (2011). Extended Theories of Gravity. Physics Reports, 509(4–5), 167–321. https://doi.org/10.1016/j.physrep.2011.09.003
32. Sotiriou, T. P., & Faraoni, V. (2010). f(R) theories of gravity. Reviews of Modern Physics, 82(1), 451–497. https://doi.org/10.1103/RevModPhys.82.451
33. Carniani, S., et al. (2024). Spectroscopic confirmation of two luminous galaxies at a redshift of 14. Nature, 633(8029), 318–322. https://doi.org/10.1038/s41586-024-07860-9
34. Weinberg, D. H., et al. (2015). Cold dark matter: Controversies on small scales. Proceedings of the National Academy of Sciences, 112(40), 12249–12255. https://doi.org/10.1073/pnas.1308716112
35. Riess, A. G., et al. (1998). Observational Evidence from Supernovae for an Accelerating Universe and a Cosmological Constant. The Astronomical Journal, 116(3), 1009–1038. https://doi.org/10.1086/300499
36. Famaey, B., & McGaugh, S. S. (2012). Modified Newtonian Dynamics (MOND): Observational Phenomenology and Relativistic Extensions. Living Reviews in Relativity, 15(1), 10. https://doi.org/10.12942/lrr-2012-10
37. Boylan-Kolchin, M., Bullock, J. S., & Kaplinghat, M. (2011). Too big to fail? The puzzling darkness of massive Milky Way subhaloes. Monthly Notices of the Royal Astronomical Society: Letters, 415(1), L40–L44. https://doi.org/10.1111/j.1745-3933.2011.01074.x
38. Schmidt, B. P., et al. (1998). The High-Z Supernova Search: Measuring Cosmic Deceleration and Global Curvature of the Universe Using Type Ia Supernovae. The Astrophysical Journal, 507(1), 46–63. https://doi.org/10.1086/306308

 doi:10.20944/preprints202509.0353.v3

39. Chen, X., et al. (2019). Intuitive derivation of the flat-disc Galactic warp structure with Classical Cepheid variables. Nature Astronomy, 3(4), 320–325. https://doi.org/10.1038/s41550-018-0686-7
40. Poggio, E., et al. (2020). Evidence for a dynamically driven warp of the Milky Way. Nature Astronomy, 4(6), 590–596. https://doi.org/10.1038/s41550-020-1017-3
41. Bekenstein, J. D. (2004). Relativistic gravitation theory for the modified Newtonian dynamics paradigm. Physical Review D, 70(8), 083509. https://doi.org/10.1103/PhysRevD.70.083509
42. Ade, P. A. R., et al. (The Simons Observatory Collaboration). (2019). The Simons Observatory: Science goals and forecasts. Journal of Cosmology and Astroparticle Physics, 2019(2), 056. https://doi.org/10.1088/1475-7516/2019/02/056